

# On The Finetuning of MLIPs Through the Lens of Iterated Maps With BPTT

Evan Dramko<sup>1</sup>, Yizhi Zhu<sup>2,3</sup>, Aleksandar Krivokapic<sup>4</sup>, Geoffroy Hautier<sup>2,3</sup>, Thomas Reps<sup>5</sup>, Christopher Jermaine<sup>1</sup>, and Anastasios Kyrillidis<sup>1</sup>

<sup>1</sup>*Department of Computer Science, Rice University, Houston, TX, USA*

<sup>2</sup>*Department of Materials Science and Nanoengineering, Rice University, Houston, TX, USA*

<sup>3</sup>*Rice Advanced Materials Institute, Rice University, Houston, TX, USA*

<sup>4</sup>*Faculty of Technical Sciences, University of Novi Sad, Novi Sad, Serbia*

<sup>5</sup>*Department of Computer Sciences, University of Wisconsin–Madison, Madison, WI, USA*

<sup>\*</sup>*Corresponding author: Evan Dramko: (ed55@rice.edu)*

## Abstract

Vital to the creation of advanced materials is performing structural relaxations. Traditional approaches built on physics-derived first-principles calculations are computationally expensive, motivating the creation of machine-learning interatomic potentials (MLIPs). Traditional approaches to training MLIPs for structural relaxations involves training models to faithfully reproduce first-principles computed forces. We propose a fine-tuning method to be used on a pretrained MLIP in which we create a fully-differentiable end-to-end simulation loop that optimizes the predicted final structures directly. Trajectories are unrolled and gradients are tracked through the entire relaxation. We show that this method achieves substantial performance gains when applied to pretrained models, leading to a nearly 50% reduction in test error across the sample datasets. Interestingly, we show the process is robust to substantial variation in the relaxation setup, achieving negligibly different results across varied hyperparameter and procedural modifications. Experimental results indicate this is due to a “preference” of BPTT to modify the MLIP rather than the other trainable parameters. Of particular interest to practitioners is that this approach lowers the data requirements for producing an effective domain-specific MLIP, addressing a common bottleneck in practical deployment.

## 1 Introduction

**Problem Domain and Background.** A central task in computational materials research is the determination of physically realizable atomic structures. This problem, often referred to as structural determination, requires identifying configurations that satisfy the thermodynamic constraints governing crystal formation. A structure is considered stable if it corresponds to a local minimum of the *Potential Energy Surface (PES)*: a function which maps the atomic coordinates together with atomic species, charge state, and environmental conditions to the total energy of the system. In most applications, all parameters other than atomic coordinates are treated as fixed, so the PES can be regarded as a function of the atomic positions alone.

Stable structures are typically identified via relaxation trajectories: gradient-based procedures that iteratively update an initial atomic configuration toward lower-energy states according to PES gradients. These gradients correspond to inter-atomic forces and are commonly computed using a physics-derived first-principles algorithm known as *density functional theory (DFT)*. While DFT provides reliable forces, each evaluation is expensive; full relaxations can take hours to days on high-performance computing systems, which makes relaxation a significant bottleneck in high-throughput materials discovery pipelines.

**MLIPs.** Machine learning interatomic potentials (MLIPs) have emerged as an alternative to running full DFT relaxation trajectories [1, 2]. These models learn to approximate DFT by taking atomic structures as input and predicting forces. Because high precision is still required in many atomistic calculations, MLIPs are commonly used as a pre-relaxation step: they cheaply move structures closer to relaxation, after which

DFT is applied for final refinement [3, 4]. Many architectural variants of MLIPs exist [4–11], but the method in this work is agnostic to the specific MLIP architecture chosen.

One of the core obstacles in training MLIPs is that each new data point demands expensive first-principles calculations, which keeps datasets far smaller and less varied than many other machine learning domains [12, 13]. Because data collection is often prohibitively expensive on scale, we introduce a work focused on improving performance by making better use of the data already available.

**Levels of Optimization.** We note that there are two levels of optimization inherent to this work: (1) optimization of the MLIP, and (2) optimization of the PES. Recall, we are training/optimizing the MLIP such that it can be used as the gradient function when we optimize along the PES. To keep these two different levels of optimization clear, we will denote training the MLIP as “local” optimization, and optimizing the structure along the PES as “global” or “PES-level” optimization.

**Defining frame.** We denote by **frame**, a single DFT/MLIP force prediction step followed by a corresponding structural update step. Without loss of generality, **frame** is expressed in Eq 1.

$$\mathbf{frame}(\mathbf{X}_t) \rightarrow \mathbf{X}_{t+1} = \begin{cases} \hat{\mathbf{y}} & = \text{MLIP}(\mathbf{X}_t) \\ \mathbf{X}_{t+1} & = \mathbf{X}_t + \eta \hat{\mathbf{y}} \end{cases} \quad (1)$$

where we denote the matrix of coordinates for the structure as  $\mathbf{X}_t$  and predicted forces as  $\hat{\mathbf{y}}$ , and  $\eta$  gives the chosen PES-level step size.

**Novel Training Approach.** Prior work trains MLIPs to match DFT forces at each structure independently. We instead adopt a trajectory-level finetuning approach: we unroll entire relaxation trajectories and apply backpropagation through time (BPTT) to update model parameters based on the quality of the final relaxed structure, rather than per-step force accuracy. This redefines the training objective as optimizing the result of the relaxation procedure directly, enabling the model to exploit trajectory-level supervision and improve performance without additional data. Figure 1 illustrates the setup. Notably, the model learns to refine its force predictions using structural information, effectively leveraging one data modality to supervise another.

**Connection to Iterative Maps.** Regardless of the use of MLIPs or DFT, we can consider PES-level optimization as a fixed point computation of the function **frame** 1. In the real world—which follows gradient flow rather than gradient descent along the PES—we are guaranteed to find a local minima. Assuming sufficiently small  $\eta$ , we observe:

$$\lim_{n \rightarrow \infty} \mathbf{frame}^n(\mathbf{X}_n) = \mathbf{X}^* \quad (2)$$

This means that stable structures are actually fixed points of the **frame** equation defining the update process between points in our trajectories. Under this view, we see that when using our BPTT procedure to finetune the model, we are actually creating **frame** as a proxy function which seeks to match fixed points and relevant basins-of-attraction to the PES.

Our primary contributions are:

1. We introduce a full trajectory, BPTT-based, fine-tuning scheme for MLIPs
2. We present ablation studies and analysis on the effect of each component in the PES-level optimization
3. We tie BPTT training to iterative maps and proxy functions
4. We validate the procedure on datasets across multiple structural domains

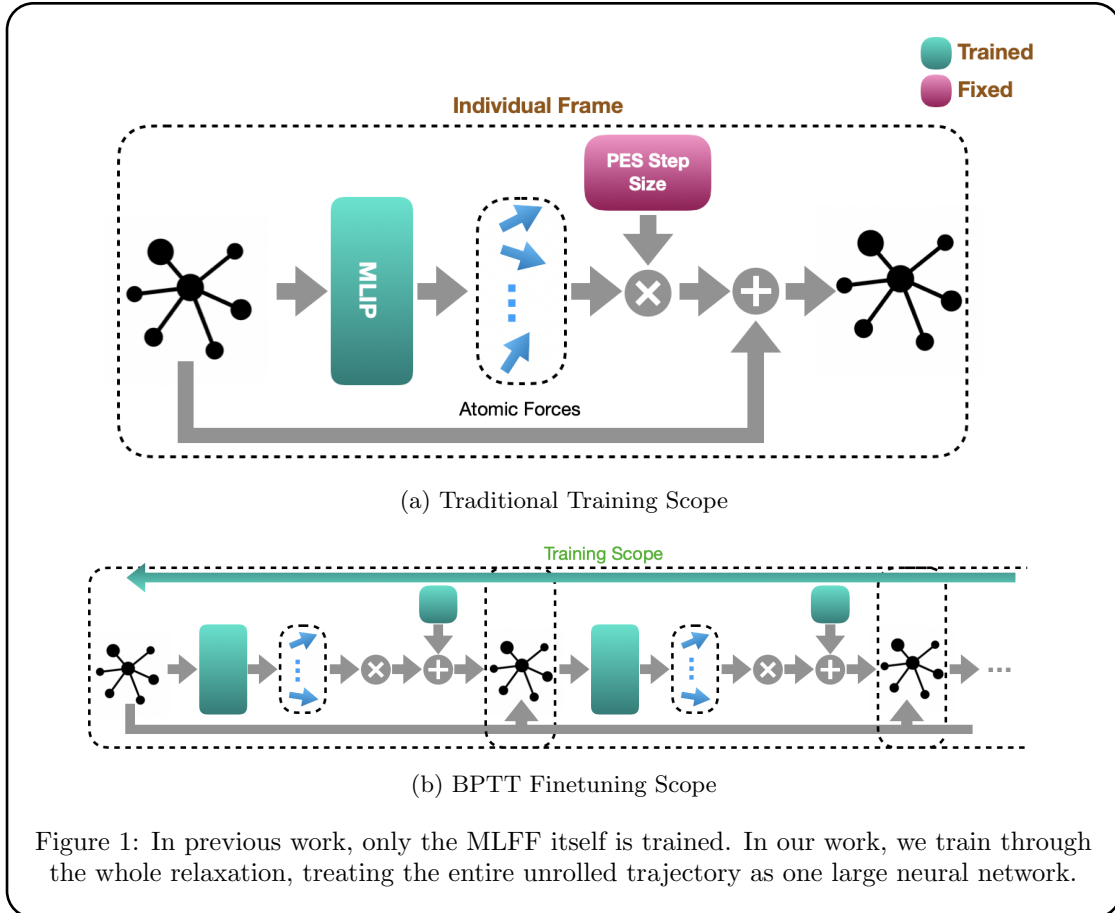
## 2 Related Works

### 2.1 MLIPs

MLIPs, also called machine learning force fields (MLFFs), are trained to take structure snapshots<sup>1</sup> and produce predictions for forces and formation energy. A dominant direction of research in MLIPs has been graph neural networks (GNNs), which have led to many of the leading architectures [5–11]. Another architecture

---

<sup>1</sup>structure snapshots: atomic locations, atomic descriptors, etc



of particular note to this paper is ADAPT [4], which uses a points-in-space representation of atoms rather than a graphical one, and uses a Transformer encoder to predict atomic forces.

Some works focused on improving MLIP performance have looked at using targeted or active learning to automatically identify areas of MLIPs that need to be trained [14–16]s.

## 2.2 Direct Structure Prediction

There has been interest in predicting relaxed states of structures directly without optimizing along the PES. Since stable structures are found through a non-convex optimization problem, data requirements for such strategies are often infeasibly high [17, 18]. One work [19], shows success for the limited domain of 2d point defects. Another approach, [20], uses an internal iterative geometry solver to create a prediction of the final structure but has not been proven in a robust manner comparable to MLIPs.

## 2.3 Iterative Approaches

Literature has explored weight-tying and iterative maps extensively [21, 22], with *deep equilibrium networks (DEQs)* [22] matching our problem domain. The majority of the research [22–24] has not been focused on the physical sciences. While such techniques have been shown to be successful under the right conditions [22, 25], they often exhibit poor training dynamics and generalizability [23, 25–27]. Due to this, they are often used in memory constrained circumstances [26, 27], and for theoretical exploration [24, 26–28]. Recent work [29] applies deep equilibrium models to predict self-consistent Hamiltonians directly, attempting to bypass the iterative SCF procedure that constitutes a major computational bottleneck in DFT.

One notably related technique from materials science literature is DOGSS [30]. This technique learns a network that creates parameters to condition a simple proxy function which matches desired physical

properties at the minima. The network’s conditioning of the proxy function is trained through the fully-differentiable gradient descent optimization of the proxy. DOGSS however, does not integrate with MLIP literature, and instead focuses on spring constants and equilibrium distances.

## 2.4 Sequence Level Work

Backpropagation through time [31–33] is the standard method for computing gradients in recurrent neural networks, and is widely used throughout sequence learning literature. It remains the conventional baseline for training RNNs and underpins most subsequent developments in recurrent and sequence-model learning.

There has been substantial work throughout machine learning on full-sequence training, often in the form of reinforcement learning from human feedback (RLHF) [34, 35]. While some aspects such as the use of proximal term weight controls [36] or gradient clipping [37, 38] overlap with our work, we differ strongly in that we have a fully-differentiable setup.

Some work, [39, 40], has used fully-differentiable training to match molecular dynamics (MD) trajectory coefficients to those observed in practice. These values are useful in many aspects of materials science, but are orthogonal to our goal of structural relaxation. Another work [41] finds BPTT unsuitable to train a specific coarse-grained molecular dynamics simulation engine<sup>2</sup>.

## 3 Method

### 3.1 Preliminaries

**Notation.** In a slight abuse of notation, we denote  $\mathbf{X}$  as the atomic structure under consideration, and also as a  $\mathbb{R}^{n \times 3}$  matrix of their coordinates. The ground truth relaxed structure is given by  $\mathbf{X}_F^*$ , and the predicted structure is  $\hat{\mathbf{X}}_F$ . We denote actual forces with  $\mathbf{y}$  and predicted forces as  $\hat{\mathbf{y}}$ .

**Evaluation: Loss and Delta Q.** Many works use MSE as a measure for structural error. However, in crystal defect cases, MSE can overemphasize the effect of the bulk lattice, and underemphasize the effect of the defect center [4]. To handle this issue, we use Delta Q (Dq) as a loss function, which is MSE where the error from each atom is weighted by its atomic mass. Given a set  $\mathbf{X}^*$  of  $n$  atoms with masses  $m_i$ , and a predicted set of atom locations  $\hat{\mathbf{X}}$ , Dq is defined by:

$$\text{Dq}(\mathbf{X}_F^*, \hat{\mathbf{X}}_F) = \sqrt{\sum_{j=1}^n m_j \|\mathbf{X}_{j,:}^* - \hat{\mathbf{X}}_{j,:}\|_2^2}, \quad (3)$$

This metric is physically meaningful and is often used in first-principles optical property computations [42].

**ADAPT Architecture Summary.** We adopt the ADAPT architecture [4] to use as our pretrained MLIP base due to both its effectiveness and its algorithmic simplicity. The model is defined as three-layer embedding MLP, a series of  $n$  Transformer encoder blocks and a final layer linear projection. Each encoder block (denoted **enc**) is given by:

$$\text{enc}(\mathbf{X}) \rightarrow \mathbf{X}_{out} = \begin{cases} \mathbf{H}_1 & = \text{LN}(\mathbf{X}_{in} + \text{Attn}(\mathbf{X}_{in})), \\ \mathbf{H}_2 & = \text{FFN}(\text{LN}(\mathbf{H}_1)), \\ \mathbf{X}_{out} & = \text{LN}(\mathbf{H}_2 + \mathbf{H}_1) \end{cases} \quad (4)$$

ADAPT also uses projection and embedding operations defined by:

$$\text{proj} = \mathbf{W}_p \mathbf{X} \quad (5)$$

$$\text{emb} = \mathbf{W}_2 \circ \sigma \circ \mathbf{W}_1 \circ \sigma \circ \mathbf{W}_0(\mathbf{X}) \quad (6)$$

---

<sup>2</sup>This engine is not a neural network, nor should it be considered neural-network-like.

where  $\mathbf{W}_p \in \mathbb{R}^{3 \times d_{model}}$ , **emb** is a multi-layer perceptron (MLP), and  $\circ$  is the function composition operator. Note that the embedding does not use a positional encoding because the coordinates of the each atom is included in the atom features given to the model. The relative ordering of atoms does not matter.

The overall ADAPT architecture is given by:

$$\text{MLIP} = \text{proj} \circ \underbrace{\text{enc} \circ \dots \circ \text{enc}}_{\times n} \circ \text{emb}(\mathbf{X}) \quad (7)$$

### 3.2 Trajectory Unrolling

In this BPTT-driven fine-tuning scheme, we unroll and train end-to-end through entire relaxation trajectories. Recalling **frame** from Eq. 1, we define a rollout<sup>3</sup> as:

$$\hat{\mathbf{X}}_{\mathbf{F}} = \underbrace{\text{frame} \circ \dots \circ \text{frame}}_{\times k}(\mathbf{X}_0) \quad (8)$$

The stopping condition is non-differentiable; it is defined as either a small  $\mathcal{L}_2$  distance between successive steps, or a maximum threshold of steps, whichever comes first. We do not train through this stopping condition, rather we take the **Dq** between the predicted and final structure as our loss metric:

$$\mathcal{L} = \text{Dq}(\mathbf{X}_F^*, \hat{\mathbf{X}}_{\mathbf{F}}) \quad (9)$$

Fundamentally, we are training the network such that:  $\text{frame}^k(\mathbf{X}_0) = \hat{\mathbf{X}}_{\mathbf{F}} \rightarrow \mathbf{X}_F^*$ . Note that  $k$  may not be the same for each rollout, meaning that we are inherently training a different function for different samples from the dataset.

Experimental results indicate that, consistent with observations from RLHF-style fine-tuning, only a small number of epochs are required to achieve meaningful improvements. Figure 3 presents outcomes obtained after five epochs of fine-tuning showing that training has stabilized.

### 3.3 PES-Level Step Size Controls

Central to any gradient descent procedure is the selection of step size. The FIRE optimizer [43] is commonly used in existing relaxation pipelines. While, the non-differentiable nature of it makes it unfit for BPTT fine-tuning, we use the pretrained force and energy models from [4] to establish a baseline result. As alternatives, we test using BPTT fine-tuning with the use of a: (1) simple scalar or (2) NN that predicts the step size.

**Scalar Step.** As a baseline, we use a grid search to establish the near optimal performance of ADAPT on the test set given perfect information. We find that a step size of 0.077 produces the best result on the test set, as seen from results in Appendix D. To establish performance of our model, we test both using a static and a learned step size. Figure 3b shows there is a negligible difference in performance when allowing backprop to change the step size. In fact, experimental results show that BPTT prefers to update the MLIP weights: in the example shown in Figure 3b, the step size was initialized to 0.50, but ended at  $\sim 0.49$  when exposed to gradient updates. Interestingly, we find even when we deviate far from the pre-computed “ideal” step size, BPTT adjusts quickly to the step size, and reaches near identical performance. This reinforces the idea that BPTT fine-tuning is learning about the interplay of the force predictions and the larger descent procedure.

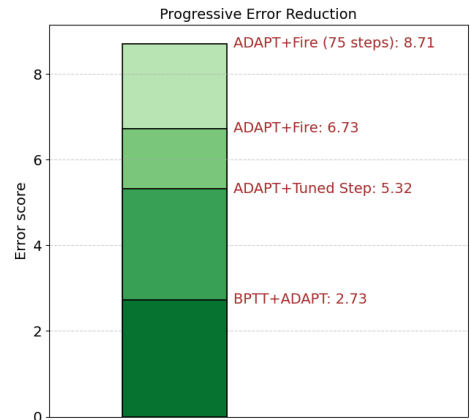


Figure 2: Effect of training schemes on Si defect relaxations

<sup>3</sup>We define trajectory length as  $k$  rather than  $T$  to avoid confusion with the transpose operator,  $\mathbf{T}$ , when the length is used as an exponent

**Neural Network Step.** We implement a single-value decoder as seen in Appendix A. This decoder uses the structure and the predicted forces as input, and predicts a PES-level step size. We test random initialization and an initialization on a model trained to always predict the value 0.077 from random noise interpolation, and find negligible difference in performance. The MLIP modifications are however tied to the PES-level step size; when using a model trained on a learned step size initialized to 0.5 in a inference time loop with a step of 0.005, the average Dq score falls to over 13.77.

Type	Avg. Dq
No BPTT	5.32
Scalar Step Size	2.73
Decoder (Single Value)	3.37

Table 1: Ablation studies on learned step sizes  
Results are from the Si defect dataset

Table 1 shows that BPTT-tuned generated trajectories outperform even the trajectories made with optimal, perfect-information step size with the untuned ADAPT. We find that using BPTT and a fixed step size yields the best overall performance, creating a  $\sim 50\%$  reduction in error over even the perfect-information untuned case.

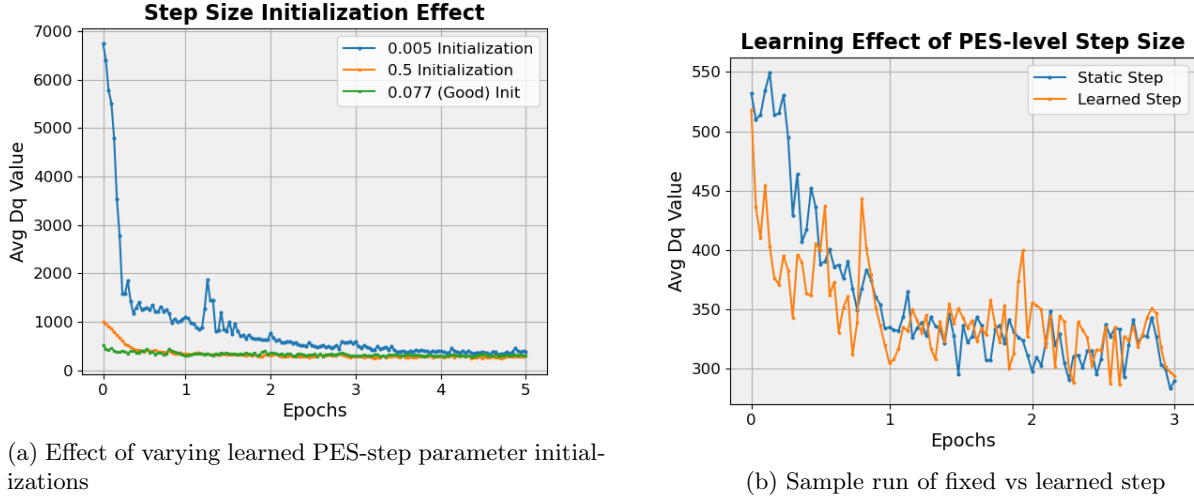


Figure 3: Experimental results comparing learned and fixed scalar step sizes as applied to Si defects.

Key takeaways from these studies are:

1. Figure 2 shows BPTT is capable of learning a step size that outperforms domain engineered optimizers,
2. Figure 3a shows that BPTT is capable of learning around a highly non-optimal step size such that the relaxations perform on par with grid-searched, perfect-information selected initial hyperparameters,
3. Figure 3 shows BPTT modifies the force predictions such that they produce better relaxed structures, even at the cost of deviating from accuracy in DFT force reproduction,
4. Table 1 shows using a neural network defined by  $S : \mathbf{X}|_{\text{cat}} \hat{\mathbf{y}} \rightarrow \text{step}$  does not outperform using a scalar or fixed step size.

### 3.4 Adaptability and Artificial Controls on Descent Dynamics

In optimization literature, pure stochastic gradient descent (SGD) is seldom employed in practice. Instead, machine learning typically utilizes step-size schedulers, momentum variants, or second-order approximations.

Domain-specific optimizers have also emerged, such as the FIRE algorithm in atomistic modeling. Noise injection—in various forms<sup>4</sup>—during training can enhance generalization. Moreover, the use of proximal weight penalties and gradient clipping helps constrain fine-tuning updates, ensuring that new policies remain close to their predecessors and mitigating catastrophic forgetting or overfitting.

Since the relaxation trajectory is inherently an optimization procedure, it is reasonable to expect that such modifications to the PES-level descent may have an impact on the BPTT-derived weight updates. Specifically, we perform ablation studies to test the effect of the PES-level application of: (1) noise injection<sup>5</sup>, (2) momentum and annealing in steps, and (3) intentional varying of trajectory lengths though modifications of stopping conditions. We also test the effect of the MLIP-level usage of proximal term vs gradient clipping update controls.

We find that none of these modifications substantively improve results, and some cause degenerative trajectories. This indicates that: (1) the model is capable of learning a strong set of optimization controls, and (2) these controls are substantively different than those we typically use. A full discussion and numeric results for each of these modifications is available in Appendix B.

## 4 Analysis and Interpretation

We explore the effect that BPTT has on the MLIP within its training loop. Experimental results in Table 2 show that BPTT reduces the accuracy in force predictions, despite Table 1 showing it improves the final structure predicted by the relaxation loop. We also include 5a showing that BPTT does not achieve meaningful gains in performance when only allowed to update the PES step size and not the MLIP. Taking these two results in combination, we assert that BPTT fine-tuning is neither improving the PES-level descent parameters nor the “physicality” of the relaxation, rather it is learning a general trend in the structural dataset. Recall that a classic MLIP is not actually solving structure relaxation, it is instead training to recreate molecular dynamics (MD) trajectories which simulate the *path* taken by the atoms. If the path is followed perfectly, then the final state will indeed be the relaxed structure. However, due to data shortages and the inherent imprecision of ML methods, we observe that often in practice the predicted relaxed state from MLIP-based MD simulations often exhibits high error [44, 45]. By using BPTT, we are creating a proxy function `frame 1` that functions as an iterative map calculation. We are simply using the MLIP as a rough initialization for that function, we are not trying to improve the descent dynamics along the PES, but rather a function that matches key properties (namely locations of fixed points) to the PES. We know that the PES must have fixed points, because DFT relaxation itself is a fixed point calculation. This approach of creating proxy functions which match key properties to first-principles calculations has been used successfully in literature under different circumstances [30].

Finding minima of the PES in inherently solving a non-convex optimization problem. Furthermore, it has been shown that structural calculations are an  $n$ -body problem, meaning that there does not exist any analytical function to represent it. Because of this, any function—including a neural network—cannot learn this system perfectly. Taken in combination, these two results indicate that molecular dynamics (i.e: gradient descent) methods are best for universal MLIPs. However, we find that BPTT is capable of imparting

Type	$\mathcal{L}_2$ Force Errors
Pretrained MLIP	4.32
BPTT-tuned MLIP	13.36

Table 2: Effect of BPTT training on force predictions for Si defects

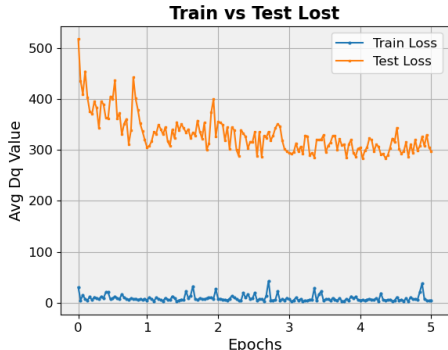


Figure 4: Si defect training loss sees negligible improvement, but testing loss is substantially improved

<sup>4</sup>Stochasticity can be seen as a form of “noise injection” as well, although we do not test a version of the model without due to compute limitations.

<sup>5</sup>Noise injection has been utilized in literature by [10]

substantive performance gains, and while it may not be solving the original physics problem directly, it does learn a function that approximates well the dataset it is given. This shows iterative maps reliably steer systems towards stable contractions, even at the expense of faithfully representing local dynamics; meaning that it forces global trends over local accuracy. In an “ideal” scenario with enough data and compute resources, local dynamics could be learned perfectly. However, we know that this is an unreasonable expectation in MLIP domains. Due to this we suggest, if possible, starting with a pretrained universal MLIP, then fine-tuning with supervised structure to force prediction, then ending with BPTT trajectory level training. While this incurs a somewhat high overhead, many researchers focus on specific types or subsets of materials (such as silicon defects), making this well worth the effort for them.

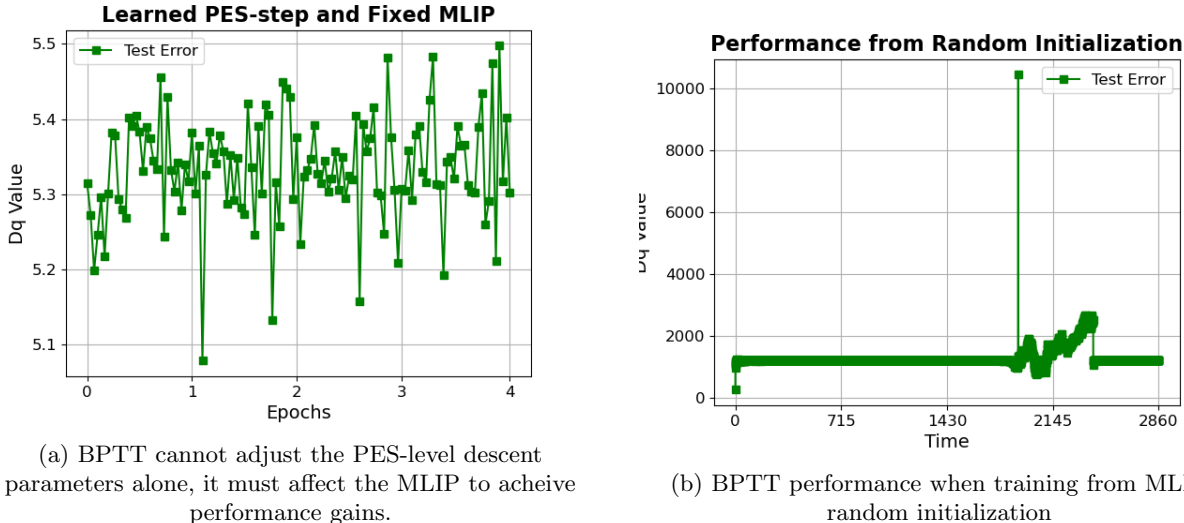


Figure 5: Effect of adjusting learning setup on Si defect samples

Our experimental results support this; Figure 5b shows that training ADAPT on the Si defect case with BPTT and random initialization is unable to find a model that exhibits strong performance. Instead, we emphasize our work as a fine-tuning measure. Under this lense, we note a similarity to *reinforcement learning from human feedback (RLHF)* literature. We can see in Figure 4 that even though the training loss remains relatively stable, the testing accuracy improves substantially. This results shows that BPTT improves generalization, mirroring results observed in RLHF literature [46, 47].

Other techniques that have shown success in directly training iterative approaches in materials science [30] do not try to train iterative neural networks, but rather create new problem setups altogether. However, DFT and MLIP literature are an established part of workflows, presenting a hurdle for such approaches.

## 5 Results

Among modern research directions in advanced materials, *crystals*—periodic, infinitely repeating arrangements of atoms known as lattices—are of particular relevance. We validate BPTT fine-tuning by testing on two different datasets which represent fundamentally different types of crystal domains. The success of BPTT fine-tuning under such different domains shows that its benefit is not limited to a specific problem scope.

### 5.1 Crystal Defects.

A central theme in materials design is the deliberate introduction of *defects*: controlled disruptions of an otherwise perfect lattice to engineer specific electrical, magnetic, or quantum properties. This dataset, sourced from ADAPT [4], focuses on point defects in silicon. Point defects occur wherever the crystal’s



regular structure is broken in a constrained local region. They are typically classified into three categories: *i*) **Substitution**: a lattice atom is replaced with a different element; *ii*) **interstitial**: an additional atom is inserted between lattice sites; and, *iii*) **vacancy**: a lattice site is missing an atom.

These seemingly simple atomic irregularities—vacancies or irregular atoms within a crystal lattice—are fundamental to modern electronic and quantum technologies. They can also combine to form defect complexes, where multiple point defects interact within the same region of the crystal. Such engineered defects are the basis of semiconductor doping for high-performance computing, and they are central to emerging efforts to create stable qubits and quantum sensors.

As summarized in Table 3, fine-tuning with BPTT produces notably improved final configurations. Qualitative analysis of the resulting defect structures shows that the defect centers—regions of greatest practical relevance—exhibit the most pronounced improvements. In particular, BPTT has a significant influence on the localization of interstitial defect atoms in the test cases. These observations confirm that the improvements are not attributable to trivial stabilization of the bulk lattice, which would be unlikely to produce a substantial reduction in the number of DFT steps required for full relaxation. It is shown in [4] that increasing the size and training time of the pretrained ADAPT model on this dataset does not improve its performance; this shows that BPTT fine-tuning is achieving accuracy in relaxations that would have been impossible with regular MLIP training.

Visual inspection of randomly selected samples from the test set shows that the defect centers exhibit noticeable improvements. Defect centers are the regions with the greatest structural evolution, and thus both the area of primary interest for scientists as well as the area which largely determines how many relaxation steps are needed. In particular, BPTT has a significant influence on the localization of interstitial defect atoms in the test cases. These observations confirm that the improvements are not attributable to trivial stabilization of the bulk lattice, which would be unlikely to produce a substantial reduction in the number of DFT steps required for full relaxation.

Type	Avg Dq
MACE + FIRE	12.59
ADAPT + FIRE	6.73
ADAPT with Step=0.077	5.25
BPTT Tuned	2.73

Table 3: Full effect of BPTT tuning

## 5.2 Pure Crystals

We consider a subset of the dataset from [8], which is itself a curation of data from the Materials Project [48]. Full details on the dataset preparation are in Appendix C.1. This contains pure crystal cells. Each cell is assumed to be subject to the periodic boundary condition, and is part of an infinitely repeating regular lattice. Due to the smaller number of atoms and lack of specific interest areas, we use standard MSE loss as our metric for this dataset. Since no pretrained version exists, we train ADAPT [4] first on first predictions, then use BPTT fine-tuning. We show that BPTT leads to a substantial increase in final-structure accuracy, as shown in Figure 6.

## 6 Discussion

We present a method for fine-tuning MLIPs that uses structure information to modify force predictions. We calculate fully-differentiable relaxation trajectories using MLIPs, and then perform a BPTT update. This work shows dramatic increases in prediction accuracy. We provide ablation studies highlighting the impact different common gradient descent schemes have when integrated into the BPTT pipeline, and find that surprisingly the algorithm is capable of adapting around a fixed scalar PES-level step size to match or outperform any other procedure.

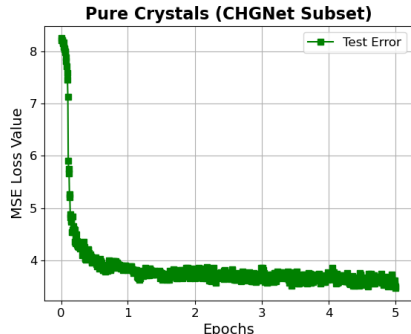


Figure 6: BPTT tuning improves pure crystal results by roughly 50%.

## References

- [1] Volker L Deringer, Miguel A Caro, and Gábor Csányi. Machine learning interatomic potentials as emerging tools for materials science. *Advanced Materials*, 31(46):1902765, 2019.
- [2] Jörg Behler. Perspective: Machine learning potentials for atomistic simulations. *The Journal of chemical physics*, 145(17), 2016.
- [3] Hugo Rossignol, Michail Minotakis, Matteo Cobelli, and Stefano Sanvito. Machine-learning-assisted construction of ternary convex hull diagrams, 2023. URL <https://arxiv.org/abs/2308.15907>.
- [4] Evan Dramko, Yihuang Xiong, Yizhi Zhu, Geoffroy Hautier, Thomas Reps, Christopher Jermaine, and Anastasios Kyrillidis. Adapt: Lightweight, long-range machine learning force fields without graphs. *arXiv preprint arXiv:2509.24115*, 2025.
- [5] Ilyes Batatia, David P Kovacs, Gregor Simm, Christoph Ortner, and Gábor Csányi. Mace: Higher order equivariant message passing neural networks for fast and accurate force fields. *Advances in neural information processing systems*, 35:11423–11436, 2022.
- [6] Chi Chen and Shyue Ping Ong. A universal graph deep learning interatomic potential for the periodic table. *Nature Computational Science*, 2(11):718–728, 2022.
- [7] Kamal Choudhary and Brian DeCost. Atomistic line graph neural network for improved materials property predictions. *npj Computational Materials*, 7(1):185, 2021.
- [8] Bowen Deng, Peichen Zhong, KyuJung Jun, Janosh Riebesell, Kevin Han, Christopher J Bartel, and Gerbrand Ceder. Chgnet as a pretrained universal neural network potential for charge-informed atomistic modelling. *Nature Machine Intelligence*, 5(9):1031–1041, 2023.
- [9] Han Yang, Chenxi Hu, Yichi Zhou, Xixian Liu, Yu Shi, Jielan Li, Guanzhi Li, Zekun Chen, Shuizhou Chen, Claudio Zeni, et al. Mattersim: A deep learning atomistic model across elements, temperatures and pressures. *arXiv preprint arXiv:2405.04967*, 2024.
- [10] Gwooon Cheon, Lusann Yang, Kevin McCloskey, Evan J Reed, and Ekin D Cubuk. Crystal structure search with random relaxations using graph networks. *Preprint at https://arxiv.org/abs/2012.02920*, 2020.
- [11] Albert Musaelian, Simon Batzner, Anders Johansson, Lixin Sun, Cameron J Owen, Mordechai Kornbluth, and Boris Kozinsky. Learning local equivariant representations for large-scale atomistic dynamics. *Nature Communications*, 14(1):579, 2023.
- [12] Bing Huang, Guido Falk von Rudorff, and O Anatole von Lilienfeld. The central role of density functional theory in the ai age. *Science*, 381(6654):170–175, 2023.
- [13] Lukas Hörmann, Wojciech G Stark, and Reinhard J Maurer. Machine learning and data-driven methods in computational surface and interface science. *npj Computational Materials*, 11(1):196, 2025.
- [14] Ganesh Sivaraman, Anand Narayanan Krishnamoorthy, Matthias Baur, Christian Holm, Marius Stan, Gábor Csányi, Chris Benmore, and Álvaro Vázquez-Mayagoitia. Machine-learned interatomic potentials by active learning: amorphous and liquid hafnium dioxide. *npj Computational Materials*, 6(1):104, 2020.
- [15] Ryan Jacobs, Dane Morgan, Siamak Attarian, Jun Meng, Chen Shen, Zhenghao Wu, Clare Yijia Xie, Julia H Yang, Nongnuch Artrith, Ben Blaiszik, et al. A practical guide to machine learning interatomic potentials—status and future. *Current Opinion in Solid State and Materials Science*, 35:101214, 2025.
- [16] Patrick WV Butler, Roohollah Hafizi, and Graeme M Day. Machine-learned potentials by active learning from organic crystal structure prediction landscapes. *The Journal of Physical Chemistry A*, 128(5):945–957, 2024.

- [17] Tom Sercu, Robert Verkuil, Joshua Meier, Brandon Amos, Zeming Lin, Caroline Chen, Jason Liu, Yann LeCun, and Alexander Rives. Neural potts model. *bioRxiv*, pages 2021–04, 2021.
- [18] Rui Shu, Hung H Bui, Shengjia Zhao, Mykel J Kochenderfer, and Stefano Ermon. Amortized inference regularization. *Advances in Neural Information Processing Systems*, 31, 2018.
- [19] Ziduo Yang, Xiaoqing Liu, Xiuying Zhang, Pengru Huang, Kostya S Novoselov, and Lei Shen. Modeling crystal defects using defect informed neural networks. *npj Computational Materials*, 11(1):229, 2025.
- [20] Ziduo Yang, Yiming Zhao, Xiaoqing Liu, Xiuying Zhang, Yifan Li, Qiujie Lyu, Calvin Yu-Chian Chen, and Lei Shen. Scaling crystal structure relaxation with a universal trustworthy deep generative model. *arXiv e-prints*, pages arXiv–2404, 2024.
- [21] Luís B Almeida. Backpropagation in perceptrons with feedback. In *Neural computers*, pages 199–208. Springer, 1988.
- [22] Shaojie Bai, J Zico Kolter, and Vladlen Koltun. Deep equilibrium models. *Advances in neural information processing systems*, 32, 2019.
- [23] Shaojie Bai, Vladlen Koltun, and J Zico Kolter. Stabilizing equilibrium models by jacobian regularization. *arXiv preprint arXiv:2106.14342*, 2021.
- [24] Christian Daniele, Silvia Villa, Samuel Vaiter, and Luca Calatroni. Deep equilibrium models for poisson imaging inverse problems via mirror descent, 2025. URL <https://arxiv.org/abs/2507.11461>.
- [25] Atish Agarwala and Samuel S Schoenholz. Deep equilibrium networks are sensitive to initialization statistics. In *International Conference on Machine Learning*, pages 136–160. PMLR, 2022.
- [26] Haixiang Sun and Ye Shi. Understanding representation of deep equilibrium models from neural collapse perspective. *Advances in Neural Information Processing Systems*, 37:9634–9667, 2024.
- [27] Mateusz Gabor, Tomasz Piotrowski, and Renato LG Cavalcante. Positive concave deep equilibrium models. *arXiv preprint arXiv:2402.04029*, 2024.
- [28] Tianxiang Gao, Xiaokai Huo, Hailiang Liu, and Hongyang Gao. Wide neural networks as gaussian processes: Lessons from deep equilibrium models, 2023. URL <https://arxiv.org/abs/2310.10767>.
- [29] Zun Wang, Chang Liu, Nianlong Zou, He Zhang, Xinran Wei, Lin Huang, Lijun Wu, and Bin Shao. Infusing self-consistency into density functional theory hamiltonian prediction via deep equilibrium models, 2024. URL <https://arxiv.org/abs/2406.03794>.
- [30] Junwoong Yoon and Zachary W Ulissi. Differentiable optimization for the prediction of ground state structures (dogss). *Physical Review Letters*, 125(17):173001, 2020.
- [31] David E Rumelhart, Geoffrey E Hinton, and Ronald J Williams. Learning representations by back-propagating errors. *nature*, 323(6088):533–536, 1986.
- [32] Paul J Werbos. Backpropagation through time: what it does and how to do it. *Proceedings of the IEEE*, 78(10):1550–1560, 2002.
- [33] Ronald J Williams and David Zipser. A learning algorithm for continually running fully recurrent neural networks. *Neural computation*, 1(2):270–280, 1989.
- [34] Paul F Christiano, Jan Leike, Tom Brown, Miljan Martic, Shane Legg, and Dario Amodei. Deep reinforcement learning from human preferences. *Advances in neural information processing systems*, 30, 2017.
- [35] Long Ouyang, Jeffrey Wu, Xu Jiang, Diogo Almeida, Carroll Wainwright, Pamela Mishkin, Chong Zhang, Sandhini Agarwal, Katarina Slama, Alex Ray, et al. Training language models to follow instructions with human feedback. *Advances in neural information processing systems*, 35:27730–27744, 2022.

- [36] Team Cohere, Arash Ahmadian, Marwan Ahmed, Jay Alammam, Milad Alizadeh, Yazeed Alnumay, Sophia Althammer, Arkady Arkhangorodsky, Viraat Aryabumi, Dennis Aumiller, et al. Command a: An enterprise-ready large language model. *arXiv preprint arXiv:2504.00698*, 2025.
- [37] John Schulman, Filip Wolski, Prafulla Dhariwal, Alec Radford, and Oleg Klimov. Proximal policy optimization algorithms. *arXiv preprint arXiv:1707.06347*, 2017.
- [38] Colin Raffel, Noam Shazeer, Adam Roberts, Katherine Lee, Sharan Narang, Michael Matena, Yanqi Zhou, Wei Li, and Peter J Liu. Exploring the limits of transfer learning with a unified text-to-text transformer. *Journal of machine learning research*, 21(140):1–67, 2020.
- [39] Joe G Greener. Differentiable simulation to develop molecular dynamics force fields for disordered proteins. *Chemical Science*, 15(13):4897–4909, 2024.
- [40] Joe G Greener. Reversible molecular simulation for training classical and machine-learning force fields. *Proceedings of the National Academy of Sciences*, 122(22):e2426058122, 2025.
- [41] Ryan K Krueger, Megan C Engel, Ryan Hausen, and Michael P Brenner. A differentiable model of nucleic acid dynamics. *arXiv e-prints*, pages arXiv–2411, 2024.
- [42] Audrius Alkauskas, Bob B Buckley, David D Awschalom, and Chris G Van de Walle. First-principles theory of the luminescence lineshape for the triplet transition in diamond nv centres. *New Journal of Physics*, 16(7):073026, 2014.
- [43] Erik Bitzek, Pekka Koskinen, Franz Gähler, Michael Moseler, and Peter Gumbsch. Structural relaxation made simple. *Physical review letters*, 97(17):170201, 2006.
- [44] Yunsheng Liu, Xingfeng He, and Yifei Mo. Discrepancies and error evaluation metrics for machine learning interatomic potentials. *npj Computational Materials*, 9(1):174, 2023.
- [45] Yifan Li, Xiuying Zhang, and Lei Shen. A critical review of machine learning interatomic potentials and hamiltonian. *Journal of Materials Informatics*, 5(4):N–A, 2025.
- [46] Binghai Wang, Rui Zheng, Lu Chen, Yan Liu, Shihan Dou, Caishuang Huang, Wei Shen, Senjie Jin, Enyu Zhou, Chenyu Shi, et al. Secrets of rlhf in large language models part ii: Reward modeling. *arXiv preprint arXiv:2401.06080*, 2024.
- [47] Zhenyu Hou, Pengfan Du, Yilin Niu, Zhengxiao Du, Aohan Zeng, Xiao Liu, Minlie Huang, Hongning Wang, Jie Tang, and Yuxiao Dong. Does rlhf scale? exploring the impacts from data, model, and method. *arXiv preprint arXiv:2412.06000*, 2024.
- [48] Anubhav Jain, Shyue Ping Ong, Geoffroy Hautier, Wei Chen, William Davidson Richards, Stephen Dacek, Shreyas Cholia, Dan Gunter, David Skinner, Gerbrand Ceder, et al. Commentary: The materials project: A materials genome approach to accelerating materials innovation. *APL materials*, 1(1), 2013.
- [49] Xuhong Li, Yves Grandvalet, and Franck Davoine. Explicit inductive bias for transfer learning with convolutional networks, 2018. URL <https://arxiv.org/abs/1802.01483>.
- [50] Chenghao Yang and Xuezhe Ma. Improving stability of fine-tuning pretrained language models via component-wise gradient norm clipping, 2022. URL <https://arxiv.org/abs/2210.10325>.

## A Scalar Decoder Head For Step Size

ADAPT provides the forces (gradient) of the PES (objective function), but does not tell us how large of a step we should take. We present a method that takes both the structure and forces as input, and outputs a step size for this iteration of the descent. This step-scaling and update procedure, **step** is defined in two parts: an upscaling projection to map from the native to embedding dimensions, and a scalar decoder head to produce a single step size for the whole structure. The scalar decoder head, **dec** is defined by:

$$\text{dec}(\mathbf{X}, \mathbf{q}) \rightarrow \hat{\mathbf{y}} = \begin{cases} \mathbf{M} = \text{MLIP}(\mathbf{X}), \\ \mathbf{h}_0 = \text{LN}(\mathbf{q} + \text{Attn}(\mathbf{q}, \mathbf{M}, \mathbf{M})), \\ \mathbf{h}_1 = \text{LN}(\mathbf{h}_0 + \text{MLP}(\mathbf{h}_0)), \\ \hat{\mathbf{y}} = \mathbf{W}\mathbf{h}_1 + \mathbf{b}. \end{cases} \quad (10)$$

where the notation follows that of Section 3.1, and dropout is applied after **Attn** and **MLP**. Recall that  $\mathbf{M} \in \mathbb{R}^{n \times d_{\text{model}}}$ , and note that  $\mathbf{W} \in \mathbb{R}^{1 \times n}$ . We use a dummy tensor  $\mathbf{q}$  of all 1s to control the dimension of the output and force it to be scalar. Although it is a matrix, we denote  $\mathbf{q} \in \mathbb{R}^{(1 \times d_{\text{model}})}$  in lower-case vector form to make clear that it has only one non-trivial dimension.

The full **step** method is given by:

$$\text{step}(\mathbf{X}) \rightarrow \mathbf{X}' = \begin{cases} \mathbf{Z} = \mathbf{X}|_{\text{cat}} \text{MLIP}(\mathbf{X}), \\ \mathbf{H} = \mathbf{W}_2 \mathbf{Z} + \mathbf{W}_1 \sigma(\mathbf{W}_0 \mathbf{Z}), \\ s = \text{dec}(\mathbf{H}), \\ \mathbf{X}' = s \cdot \text{MLIP}(\mathbf{X}) + \mathbf{X} \end{cases} \quad (11)$$

Where  $\mathbf{W}_2 \in \mathbb{R}^{d_{\text{model}} \times 15}$  and if  $d_{\text{model}} = 15$  then  $\mathbf{W}_2 = I$ .

## B Ablation Studies

### B.1 Exploration Noise

A common technique used in sequence fine-tuning tasks is the addition of noise into model weights or update steps with the intention to force the model to explore weights. Such noise is usually annealed over epochs, as the goal of the model shifts from exploration to exploitation. We conduct studies on the effect of noise in our BPTT approach, and find that it leads to vastly diminished results, even performing worse than the original model before the fine-tuning. This is a surprising result given the findings of [10] which claims that noise injection improves overall performance.

### B.2 Proximal Term vs Gradient Clipping

Often when performing fine-tuning tasks, a proximal  $\mathcal{L}_2$ -loss term anchoring the model weights to the pretrained version is added to ensure that the model does not stray too far and overfit [49]. Other have proposed using aggressive gradient clipping as an alternative [50]. Our experiments find there is a negligible performance difference between the two approaches. We adopt the gradient clipping because it is more computational lighter compared to the proximal-term approach.

### B.3 Use of Momentum and Step Annealing

Applying a momentum term to the descent term of ADAPT without BPTT yields improved results. Similarly, using a multiplicative annealing—such as  $0.99^k$  on step  $k$ —yields beneficial results. In Table 4, we report experimental results investigating the effect that these two changes produce when added into the BPTT descent trajectories. We note that the initialization value for the scalar step size hyperparameter is 0.5.

Setup	Avg Dq
ADAPT	8.47
ADAPT+Momentum	7.67
ADAPT+Anneal	7.28
ADAPT+Momentum+Anneal	7.49
BPTT	2.73
BPTT+Momentum	3.47
BPTT+Anneal	1928.30
BPTT+Momentum+Anneal	1969.71

Table 4: Characterizing the effect of momentum weight of 0.05 and  $0.99^k$  annealing-step factor on step  $k$ .

## B.4 Intentional Modification of Trajectory Length

During the training process, different examples may run for different numbers of steps. Recalling the view of this problem setup as a deep neural network made of a repeated block, this differing numbers of block instances means that we are optimizing for an inherently different situation in each example. To establish the impact of such potential mismatches, we present experiments in which we artificially vary the stopping threshold after each batch of training. In previous experiments, a threshold of 0.001 in total root mean squared error (RMSE) atomic movement across the structure is used, with a maximum of 75 steps being allowed. Under this new paradigm, we randomly varied the threshold between 0.01 and 0.0001, and randomly varied the maximum number of frames between 50 and 75. Results from this are presented in Table 5, and show that such a training setup leads to slightly worse results. The hope of this training scheme—now disproved—is that it would worsen results on the training set, but could force better generalization and improve test set performance.

Stopping Condition	Avg Dq
Fixed	2.92
Variable	3.19

Table 5: Characterizing the effect of varying stopping conditions

# C Hyperparameters and Reproducibility

Unless otherwise noted in Section B.4 or Section B.3, results are from trials using an RMSE threshold of 0.001. We impose a maximum of 75 frames in a trajectory for the Si defect case, and a maximum of 45 frames per trajectory for the pure crystals case.

## C.1 CHGNet Pure Crystals Data Subset

We use the dataset curation from CHGNet [8]. To avoid prohibitively large runtimes, we select the first 20,101 examples as the dataset. Matching to the quantities set in [4], we use the first 100 trajectories as testing data and the rest as training data. Pure crystal trajectories are often much shorter than those from defects, so we use a substantially larger quantity to create a dataset of similar number of frames to that of the silicon defects from [4]. The MLIP is first trained on the structure-force pairs from the flattened 20,001 training trajectories. After, the model is finetuned using BPTT on the 16,984 trajectories of length greater than two with constant atom counts throughout the trajectory. Finally, testing results on the 96 of the 100 test trajectories are reported, four trajectories (sequentially trajectories 15, 17, 19, 63) has mismatched atom counts throughout the trajectory in the dataset, and were thus discarded.

## D ADAPT Optimal PES Step

In Table 6 we show the average testing Dq for selected values of the PES-level step size. Notably, comparing BPTT against one of these values unfairly disadvantages BPTT because BPTT has no knowledge of the the test set, whereas these hyperparameters are fit directly on the test set.

Table 6: Hyperparameter Values for PES-Level Descent of ADAPT

Step Size	Avg Dq
0.001	12.38
0.005	9.88
0.007	9.15
0.009	8.61
0.011	8.23
0.013	7.90
0.015	7.63
0.017	7.46
0.019	7.29
0.021	7.16
0.025	6.90
0.029	6.71
0.033	6.49
0.037	6.35
0.039	6.27
0.045	6.05
0.049	5.91
0.063	5.42
0.067	5.38
0.071	5.33
0.073	5.34
0.075	5.33
0.077	5.32
0.079	5.37
0.081	5.41
0.083	5.40
0.085	5.40
0.087	5.45
0.091	5.35
0.095	5.37
0.15	9.18
0.25	20.46